This is a postprint of a published paper, in "Applied Physics Letters" by AIP publishing
available at: https://doi.org/10.1063/5.0005299
DOI: 10.1063/5.0005299

An anomalous wave formation at the Al/Cu interface during magnetic pulse welding

J.S. Li[1,*], R.N. Raoelison[2], T. Sapanathan[3], Z. Zhang[4], X.G. Chen[4], D. Marceau[4], Y.L. Hou[5,**], M. Rachik[1]

[1] Laboratoire Roberval, FRE UTC-CNRS 2012, Alliance Sorbonne université, Université de Technologie de Compiègne, Centre de recherche Royallieu, CS 60319, 60203 Compiègne cedex, France
[2] Université de Bourgogne Franche-Comté - UTBM, Laboratoire Interdisciplinaire Carnot de Bourgogne, UMR 6303 CNRS, 90100 Belfort, France
[3] UCLouvain, Institute of Mechanics, Materials and Civil Engineering, 1348 Louvain-la-Neuve, Belgium
[4] Aluminium Research Centre-REGAL, University of Quebec at Chicoutimi, Chicoutimi, QC, G7H 2B1, Canada
[5] School of Mechanical and Power Engineering, Zhengzhou University, Science Road 100, 450001 Zhengzhou, China

Corresponding author: * Jishuai. Li (jishuai.li@utc.fr)
** Yuliang Hou (yulianghou@zzu.edu.cn)

Abstract:

This paper reports an anomalous wave formation at an Al/Cu bimetallic interface produced by magnetic pulse welding. The mechanism of the anomalous wave formation is investigated using both metallurgical characterization and the interface kinematics. It reveals that the anomalous wave is formed with the combination of the intermediate zone and the interdiffusion zone with the thickness of 70 nm. Wherein, the intermediate zone is caused by the local melting due to the high shear instability and the interdiffusion zone is formed below the melting point of aluminum combined with ultrahigh heating and cooling rates of about 10^{13} ℃ s−1. A multiphysics simulation of impact welding has been performed, and it is identified that the jetting kinematics and non-uniform distribution of shear strains during high-speed collision, enable the formation of the anomalous wave. The numerical and experimental results comprehensively lead to understand the mechanism and the characteristics of the anomalous wave produced during an impact welding.

Manuscript:

Magnetic pulse welding (MPW) is regarded as a potential technology in automobile and aerospace industries due to its large production, flexibility and capability to join dissimilar lightweight metals [1,2]. Generally, the MPW process is completed within 50 μs (first half cycle of the impact current with the frequency of 10 kHz) while the interface is subjected to an incredible high-strain rate of up to 10^6–10^7 s^{-1} [3]. Thus, it is foreseeable that a complex kinematics and thermo-mechanical kinetics occur at the interface during the instantaneous high-speed collision. According to the previous studies, various interface phenomena are observed during the welding process, namely, jetting and ejection[4,5], wave and vortices [6–8], interfacial shearing [9,10], and porous structure [11–13].

Wavy interfaces are undoubtedly the most distinctive features of MPW and are generally regarded as an indication of a successful weld [14]. The wave formation mechanism is one of the most intriguing subjects to researchers over the past few decades. Experimental and numerical methods have been used to understand the wave formation during MPW in earlier studies and the main findings can be summarized as three mechanisms: (1) jetting [15]; (2) local melting and solidification [16]; (3) high shear instability [7,17,18] . Although ample work has been dedicated to regular wave formation, there was no attention given to the physical phenomena and kinematics of irregular waves. Irregular waves reveal anomalous features arising at the interface. The absence of research on such irregular anomalous wave formation is mainly due to the difficulties in characterizing the wave formation by insitu experimental methods, and challenging to predict irregular waves via numerical simulations due to dynamic and transient process conditions. In this study, we present an anomalous wave formation and investigate

using numerical simulation to elucidate the formation mechanism of the wave.

Welding tests were carried out on a tubular assembly using a single turn coil with a fieldshaper, connected to a PULSAR MPW unit with the specification of 25kJ-9kV. The experimental tests were carried out with an input voltage of 6 kV and the initial gap of 1.64 mm between the flyer and rod consist of AA6061-T6 and pure copper, respectively. Further details of the MPW process can be found in our previous studies [19]). A representative 2D thermo-mechanical model based on Eulerian formulation was used to identify the anomalous wave formation and to investigate the physical mechanism and thermo-mechanical kinetics. Johnson-Cook model was used to describe the constitutive behavior of materials under high strain rate deformation. Moreover, Grüneisen state equation was used to compute the pressure distribution for those interfacial elements where the wave formation occurs. The governing equations, material model and input parameters used for the thermo-mechanical model are provided in Supplementary Material. The Eulerian model has the same size with the experimental setup (see Fig. S1 in Supplementary Material). The electromagnetic-mechanical coupled simulations were performed using LS-DYNA® numerical package with the solver version R8 to obtain the input velocity used in the Eulerian model [20]. The obtained input velocity follows the trend described by the Eq. (1)

$$\left|V_y\right| = -300 - 70\,000x; \forall x \in [0, 0.0026] \qquad (1)$$

where, $|V_y|$ is the impact velocity perpendicular to the surface of the inner rod (Unit: m/s), and x is the distance opposite to the welding direction (from the end to the onset of welding) (Unit: m).

A scanning electron microscope (SEM) observation of the distinctive anomalous wave at

the Al/Cu interface, reveals the irregular features in terms of the wavelength and amplitude (Fig. 1a). The wave propagation direction of the anomalous wave is consistent with the welding direction. Moreover, there exists some trapped intermediate zones (IMZs) along the interface, bounded within the front of wave zone or exposed at the bimetallic welded interface. The thickness of the IMZs varies in the range of [3 m, 20 m]. Fig. 1b shows the inner architecture of IMZs revealing nanoscale porous structures. Transmission electron microscope (TEM) observations were further used to unravel the metallurgical changes and the bonding mechanism at the interface with the absence of IMZ along the anomalous wave, in the SEM observation (marked by red rectangle in Fig. 1a), and the results are presented in Figs. 1c-g. A thin layer of third material with the width of 30 nm was observed at the interface (Fig. 1c). The selected area electron diffraction (SAED) pattern (Fig. 1d) taken from this thin layer (region D in Fig. 1c) shows the diffuse halo and confirms that the third layer consist of amorphous phase (AP). The SAED patterns corresponding to the TEM observations from the aluminum and copper sides adjacent to the interface (regions E and F in Fig. 1c, respectively) exhibit the Debye ring diffraction indicative of nanocrystalline features (Figs. 1e and f). The energy dispersive spectroscopy (EDS) analysis in Fig. 1g presents an obvious gradual interdiffusion of Al and Cu elements across the interface. One should note that the interdiffusion zone having the width of ~70 nm (Fig. 1g) is slightly broader than the width of the amorphous layer (i.e. ~30 nm) in the Cu-rich side. This observation suggests that there is a possible formation of supersaturated solid solution in the Al-rich side.

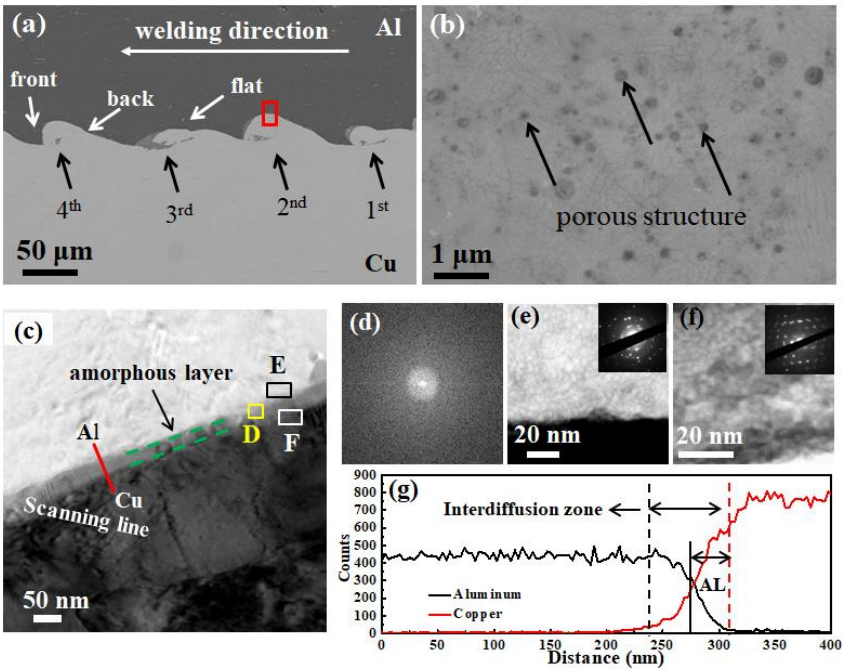

Fig. 1. (a) SEM observation showing an anomalous wave interface from Al/Cu weld, (b) SEM image of inner porous architecture of IMZs, (c) TEM observation taken from the wave interface indicated by the red rectangle in (a); TEM images and selected area electron diffraction (SAED) patterns in (d), (e) and (f) correspond to regions D, E, F marked in (c); (g) EDS revealing the distribution of Al and Cu along the red line marked in (c).

Finite element simulation is used here to elucidate the observed phenomena in the anomalous wave interface. The predicted interface morphology from Eulerian simulation given in Fig. 2a, clearly shows the accuracy in terms of the shape, size and the continuous development of the anomalous wave. Analogously flat region (3^{rd} wave) is noticed in the anomalous wave (Fig. 1a), which spreads for a length of approximately 87 μm, also well predicted in the simulation (Fig. 2a). Fig. 2b illustrates the computed temperature field of the interface, revealing the local heating due to the confined plastic deformation. Moreover, the temperature rise in the interface regions makes it reaches above both melting temperatures of Al and Cu (~ 660 ℃ and ~ 1085 ℃, respectively), enabling a rapid local melting and solidification that could result in the formation of the IMZs. This prediction is also in good agreement with the shape and occurrence site of the experimentally observed discontinuous IMZs along the interface (Fig. 1a). The predicted temperature and deformation histories of

the interface are depicted in Fig. 2c to further understand the thermo-mechanical conditions that facilitate the interface diffusion and the AP formation. Temperature and pressure curves shown in Fig. 2c are obtained from the point ①, indicated in Fig. 2e, corresponding to the TEM sample location. Upon the collision process, the wave interface experiences a rapid temperature rise with an ultrahigh heating rate of ~10^{14} ℃ s^{-1}. Then, the temperature continues to hoist up to 643 ℃ simultaneously until the pressure reaches the maximum value of 6.5 GPa. The temperature of point ① does not exceed the melting point of Al and it indicates that the amorphization process is a solid-state transformation. The rise of the impact pressure induces the increase of the plastic strain at the interface and it has been accommodated via structural defects, resulting from the relatively high free surface energy. That is, as the strain exceeds a critical value, the crystal structure could collapse and transform to a crystalline-amorphous interface to reduce the surface free energy [21]. The propagation of the crystalline-amorphous interface requires atomic mobility, which is promoted by the heat generation combined with the severe plastic deformation during the high-pressure impact. The cooling rate obtained from the Eulerian simulation (Fig. 2f) also indicates that the cooling rate at the beginning (~10^{13} ℃ s^{-1}) provided the favorable condition for the formation of amorphous layer. Although, temperature prediction point is chosen to match the TEM sample location, there is a high possibility for small deviations as the TEM samples are taken from a very small region. However, the surrounding zone of point ① revealing higher cooling rates than the critical cooling rate of amorphization for aluminum liquid (10^9 Ks^{-1}) reported in literature (see for e.g. [17]), that ensures the perdition point collaborate well with the corresponding experimental observation. Based on these

observations, the anomalous wave interface is mainly formed due to two bonding mechanisms, i.e., local melting of Al at those places with the temperature above 660 ℃ and solid-state bonding elsewhere.

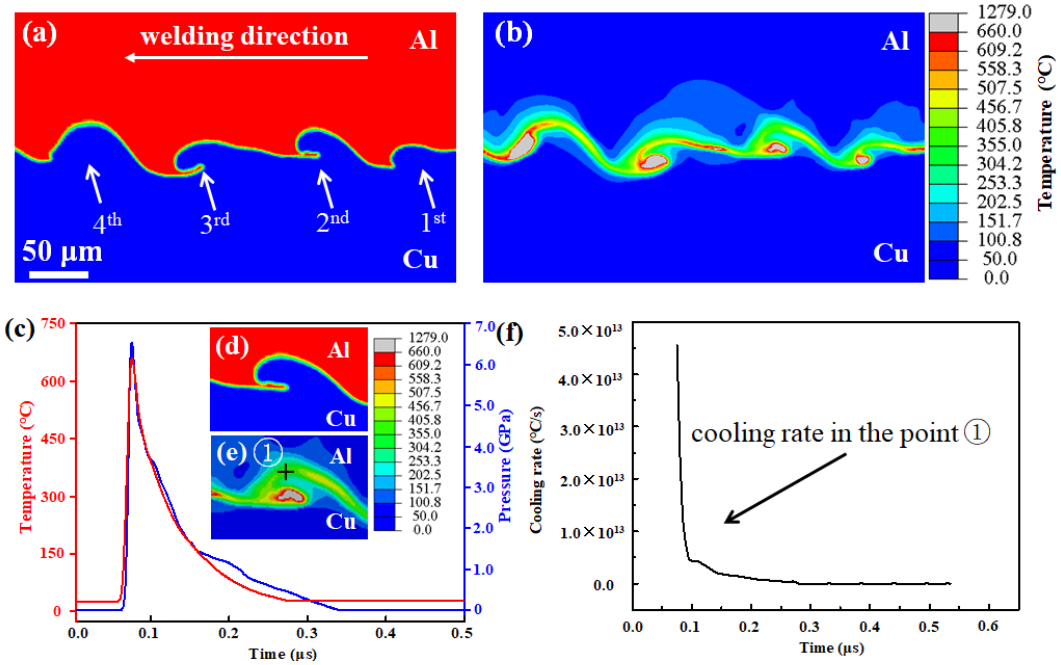

Fig. 2. (a) Anomalous wave morphology obtained from Eulerian simulation, (b) the predicted temperature distribution along Al/Cu interface. (c) The time-dependent temperature and pressure obtained from point ① (marked in inset e) in the wave morphology (d) and (e) the temperature field map and the color legend corresponding to the temperature in ℃. (f) The cooing rate obtained from point ① in (e).

From a thermodynamic point of view, the metallurgical changes occurring at the interface reveal non-equilibrium conditions, thus a complex kinematics would have happened as the anomalous wave propagates. Therefore, the detailed formation process of this anomalous wave is provided as follows. During the oblique collision, the strong interfacial shear instability arises from a tangential velocity, which produces the upward jetting (Fig. 3a and b). Then, the upward jetting interacts with an earlier protrusion emerging from the inner rod. Moreover, the flyer subjected to the impact velocity impinges onto the inner rod. The above two behaviors result in the downward jetting (Fig. 3c and d). These upward and downward jetting produce the sequence of inverted curves along the interface and form a

regular wavy pattern at the onset of collision (Fig. 3a-d). The simulation also provides an excellent description on the development of the flat interface morphology (Fig. 3e-f). In this case, the interaction angles of α and β (see Fig. 3m) are equal, thus the condition results in an unfavorable plastic deformation for the wave formation [22], and jetting always propagates parallel to the interface. Synchronously, the former regular waves continue to grow due to the increase of shear instability at their front and back sides, and eventually form the first two anomalous waves with the irregular morphology. As the collision progresses along with the increase of both deformation of materials and shear instability, the depression zone becomes larger and squeezed. In comparison with the former waves, the impact condition makes α higher than β, and it favors to produce the irregular shape (Fig. 3i-l). These flat and irregular waves together constitute the anomalous waves as shown in Fig. 1a and 2a.

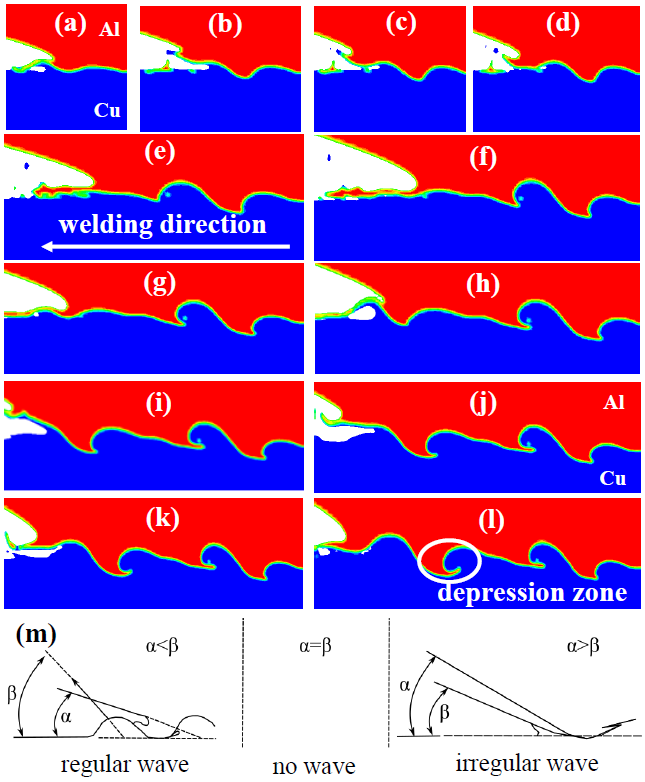

Fig. 3. Sequential development of anomalous wave obtained from Eulerian simulation: (a-d) the onset of regular wave and (e-f) the propagation of the flat wave and the first two waves; (g-l) the development of subsequent waves, (m) schematic illustration showing the interaction angles α and β during the interface wave development.

The wave development kinematics is highly related to the shear instability of the interface. Hence, the temporal and spatial variations of the interfacial shear strain development during the collision are further investigated to understand their contribution on the formation of the anomalous wave. The shear strain field around the anomalous wave is shown in Fig. 4a. It reveals that the shear strain is successively accommodated into tensile and compressive plastic strains at the front side and back side of each wave, respectively. The alternating tensile and compressive shear strain patterns are influenced by the inversion of the jetting from upward to downward directions (Fig. 3a-l). Fig. 4b presents the time-dependent variations of the tensile and compressive strains at the 2^{nd} wave (marked in Fig. 2a). The tensile and compressive strains have the same increasing trend, while the maximum compressive strain (~2.05) is much higher than that of tensile strain (~1.60). This indicates that Al side (i.e. compressive strain side) experiences much higher plastic deformation than Cu side.

The maximum tensile and compressive strains of each wave are obtained to clearly explore the relationship between the shear strain and wave pattern, plotted in Fig. 4c. Interestingly, the compressive strains of the 1^{st} and 3^{rd} waves are relatively smaller than their tensile strains, and it also explains the appearance of the flat interface in the back side of those waves (see Fig. 1a). Large tensile strain is also observed in the front side of the 3^{rd} wave than those of the other three waves, providing the interpretation of the emergence of IMZ at the bimetallic interface. To further understand the influence of the shear strain on the wave formation, the same input velocity was used to simulate the welding process of an Al/Al interface. A regular wave morphology (see Fig. S2 in Supplementary Material) was obtained.

The corresponding shear strain map of the Al/Al interface is depicted in Fig. 4d. It can be noticed that the compressive strains exhibit a higher value and distributed across a larger area than the tensile strains for the 2nd and 4th anomalous waves (Fig. 4a). While the regular waves show lower compressive shear strains (maximum of 0.82) within a larger area and higher tensile shear strains (maximum of 1.36) within a relatively smaller area. Therefore, the deformation of the Al/Cu pair and the flow behavior of front and back sides of the waves are not symmetrical compared to the Al/Al case under the same welding parameters. Thus, the condition of dissimilar interface favors to form the anomalous wave.

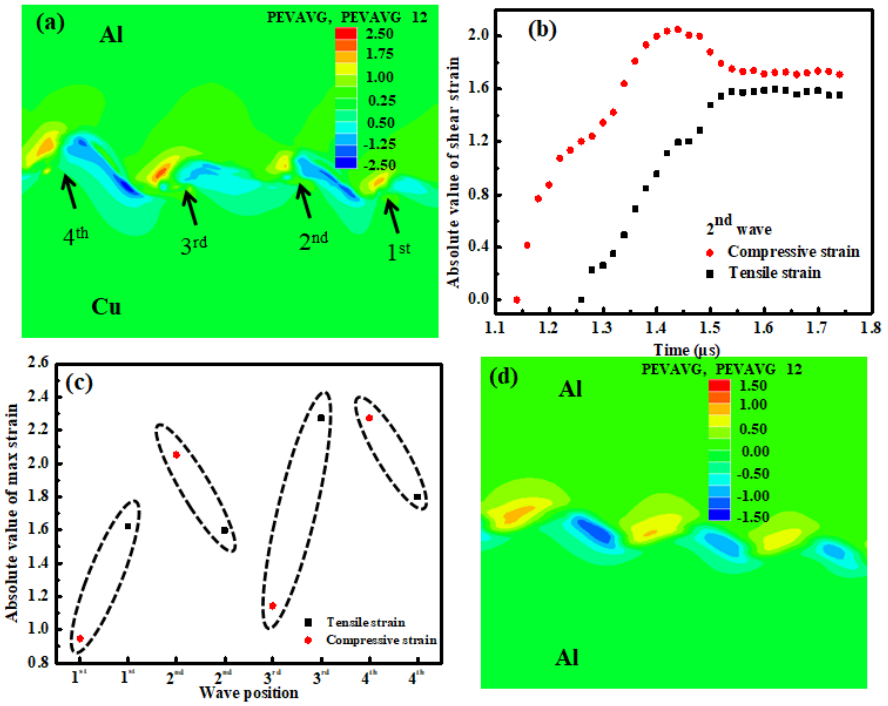

Fig.4. (a) The predicted shear strain distribution along the Al/Cu interface obtained for the anomalous wave; (b) time-dependent variations of shear strain for the 2nd wave; (c) the maximum tensile and compressive strains of each wave; (d) predicted shear strain distribution along an Al/Al interface with the same welding parameters, which resulting to form regular wave given in Fig.S1 in Supplementary material. [positive and negative values indicate the tensile and compressive stains respectively in the strain field maps in (a) and (d)].

In summary, an anomalous wave formation is investigated in a magnetic pulse welded Al/Cu interface through experimental and numerical approaches. The anomalous wave interface is formed with the combination of the intermediate zone and the interdiffusion zone.

The intermediate zone is formed due to the melting resulting from the high shear instability, while the interdiffusion zone is caused by the mechanical lattice instability due to the high-pressure impact combined with ultrahigh heating and cooling of 10^{13} ℃ s^{-1}. Thermo-mechanical simulations reproduced the complex interfacial kinematics due to the shear instability, including the jetting kinematics and non-uniform distribution of the tensile and compressive strains at the front and back sides of each wave. Moreover, the shear instability leads to produce extremely confined heating along the anomalous wave interface, resulting in those melting zones, which concur with the experimentally observed intermediate zones in terms of the location, size and shape. Thus, overall observations clarify the interfacial characteristics and the governing mechanism for the development of an anomalous wave and the formation of amorphous phase, which merits to be further investigated.

See the **supplementary material** for the details of the thermo-mechanical model and a regular wave morphology obtained for Al/Al MPW interface.

This work is supported by Co-operation Program of UTs and INSAs (France) and funded by China Scholarship Council (No. 201701810138). T. Sapanathan acknowledges F.R.S – FNRS (Belgium) during his postdoc at UCLouvain.

The data that support the findings of this study are available from the corresponding author upon reasonable request.

References

[1] A. Kapil and A. Sharma, J. Clean. Prod. **100**, 35 (2015).

[2] K. Faes, I. Kwee, and W. De Waele, Metals (Basel). **9**, (2019).

[3] J.S. Li, T. Sapanathan, R.N. Raoelison, Z. Zhang, X.G. Chen, D. Marceau, A. Simar, and M. Rachik, Mater. Lett. **249**, 177

(2019).

[4] R.N. Raoelison, T. Sapanathan, N. Buiron, and M. Rachik, J. Manuf. Process. **20**, 112 (2015).

[5] A. Stern, O. Becher, M. Nahmany, D. Ashkenazi, and V. Shribman, Weld. J. **94**, 257s (2015).

[6] J. Cui, G. Sun, G. Li, Z. Xu, and P.K. Chu, Appl. Phys. Lett. **105**, 1 (2014).

[7] R.N. Raoelison, T. Sapanathan, E. Padayodi, N. Buiron, and M. Rachik, J. Mech. Phys. Solids **96**, 147 (2016).

[8] H. Geng, Z. Xia, X. Zhang, G. Li, and J. Cui, Mater. Charact. **138**, 229 (2018).

[9] X. Jiang and S. Chen, Weld. World **62**, 1159 (2018).

[10] Y. Zhang, S.S. Babu, and G.S. Daehn, J. Mater. Sci. **45**, 4645 (2010).

[11] R.N. Raoelison, J. Li, T. Sapanathan, E. Padayodi, N. Buiron, D. Racine, Z. Zhang, D. Marceau, and M. Rachik, Materialia **5**, (2019).

[12] H. Yu, Z. Xu, Z. Fan, Z. Zhao, and C. Li, Mater. Sci. Eng. A **561**, 259 (2013).

[13] T. Sapanathan, R.N. Raoelison, N. Buiron, and M. Rachik, Scr. Mater. **128**, 10 (2017).

[14] E. Uhlmann, L. Prasol, and A. Ziefle, Adv. Mater. Res. **907**, 349 (2014).

[15] T. Sato, K. Kawauchi, and A. Muto, Weld. Int. **12**, 619 (1998).

[16] A. Ben-Artzy, A. Stern, N. Frage, and V. Shribman, Sci. Technol. Weld. Join. **13**, 402 (2008).

[17] H. Geng, J. Mao, X. Zhang, G. Li, and J. Cui, Mater. Lett. **245**, 151 (2019).

[18] A. Nassiri, A. Vivek, T. Abke, B. Liu, T. Lee, and G. Daehn, Appl. Phys. Lett. **110**, (2017).

[19] J. Li, R.N. Raoelison, T. Sapanathan, G. Racineux, and M. Rachik, Procedia Manuf. **29**, 337 (2019).

[20] T. Sapanathan, R.N. Raoelison, N. Buiron, and M. Rachik, Join. Technol. (2016).

[21] Z. Fan, H. Yu, and C. Li, Scr. Mater. **110**, 14 (2016).

[22] V.I. Lysak and S. V. Kuzmin, J. Mater. Process. Technol. **212**, 150 (2012).